Phase relations in $K_xFe_{2-y}Se_2$ and the structure of superconducting $K_xFe_2Se_2$ via high-resolution synchrotron diffraction

Daniel P. Shoemaker,[1] Duck Young Chung,[1] Helmut Claus,[1] Melanie C. Francisco,[1] Sevda Avci,[1] Anna Llobet,[2] and Mercouri G. Kanatzidis[1,3,*]

[1] *Materials Science Division, Argonne National Laboratory, Argonne, IL, 60439, USA*
[2] *Los Alamos National Laboratory, Lujan Neutron Scattering Center, MS H805, Los Alamos, New Mexico 87545, USA*
[3] *Department of Chemistry, Northwestern University, Evanston, Illinois 60208, United States*

Superconductivity in iron selenides has experienced a rapid growth, but not without major inconsistencies in the reported properties. For alkali-intercalated iron selenides, even the structure of the superconducting phase is a subject of debate, in part because the onset of superconductivity is affected much more delicately by stoichiometry and preparation than in cuprate or pnictide superconductors. If high-quality, pure, superconducting intercalated iron selenides are ever to be made, the intertwined physics and chemistry must be explained by systematic studies of how these materials form and by and identifying the many coexisting phases. To that end, we prepared pure $K_2Fe_4Se_5$ powder and superconductors in the $K_xFe_{2-y}Se_2$ system, and examined differences in their structures by high-resolution synchrotron and single-crystal x-ray diffraction. We found four distinct phases: semiconducting $K_2Fe_4Se_5$, a metallic superconducting phase $K_xFe_2Se_2$ with x ranging from 0.38 to 0.58, an insulator $KFe_{1.6}Se_2$ with no vacancy ordering, and an oxidized phase $K_{0.51(5)}Fe_{0.70(2)}Se$ that forms the PbClF structure upon exposure to moisture. We find that the vacancy-ordered phase $K_2Fe_4Se_5$ does not become superconducting by doping, but the distinct iron-rich minority phase $K_xFe_2Se_2$ precipitates from single crystals upon cooling from above the vacancy ordering temperature. This coexistence of metallic and semiconducting phases explains a broad maximum in resistivity around 100 K. Further studies to understand the solubility of excess Fe in the $K_xFe_{2-y}Se_2$ structure will shed light on the maximum fraction of superconducting $K_xFe_2Se_2$ that can be obtained by solid state synthesis.

PACS numbers: 74.70.Xa 61.05.cp 64.75.Ef

INTRODUCTION

The brief history of iron chalcogenide superconductivity has seen a flurry of activity, beginning with the discovery of T_c = 8 K in β-FeSe,[1] and later the announcement that ternary intercalated compounds in the $A_xFe_{2-y}Se_2$ system display $T_c \approx 30$ K when A is K, Rb, Cs, or Tl. [2, 3]. Much like the superconducting iron arsenides, these compounds form the $ThCr_2Si_2$ structure-type with layers of tetrahedrally-coordinated Fe and are in the vicinity of antiferromagnetism, but the differing anion charges (formally Se^{2-} versus As^{3-}) lead to issues of chemical stability that have a profound effect on the structures and properties. While arsenides are only known to exhibit superconductivity in the fully-occupied $ThCr_2Si_2$ structure type without vacancies, the hallmark of the selenides (intercalated and not) is that stoichiometry is never exact for superconducting samples—some disorder is always present, often in conjunction with phase separation. [4–7]

Experimental efforts to understand superconductivity in iron selenides must grapple with the sensitive stoichiometry required to observe T_c. Compared to iron pnictides, where a superconducting dome appears from x = 0.2 to 1 in $Ba_{1-x}K_xFe_2As_2$ for example, [8] in β-$Fe_{1+\delta}Se$ there is only a window of δ = 0.01 to 0.03 where superconductivity is observed, and there is no such dome versus composition.[9] No dome is present in $A_xFe_{2-y}Se_2$ superconductors either, with T_c approximately invariant around 30 K. [10–12] Additionally, the thermal history of the sample plays a key role, as even moderate thermal annealing has an effect on the sharpness of the transition in $A_xFe_{2-y}Se_2$. [13, 14]

Divalent Se^{2-} leads to the presence of alkali and iron vacancies that are not found in the iron arsenides. In fact, most attention in the $K_xFe_{2-y}Se_2$ system is focused on $K_{0.8}Fe_{1.6}Se_2$, shown in Figure 1. This compound is a Mott insulator with 1/5 ordered Fe vacancies and disordered K, and can be written as $K_2Fe_4Se_5$ with valence-precise Fe^{2+}. [15] Due to prevalent vacancies and the ability of Fe to adopt +2 or +3 formal oxidation states, (as in $Fe^{2+}Se$ or $KFe^{3+}Se_2$ [16]) it may seem that doping either cation in $K_xFe_{2-y}Se_2$ would tune T_c as in the arsenides, but this is not the case: the superconducting transition appears and disappears abruptly, and does not shift.[10]

A synthetic route to pure superconducting $K_xFe_{2-y}Se_2$ phases is elusive. Microscale phase separation between closely-related structures, mobile Fe/K vacancies, and iron impurities are widespread. [2, 17–22] As a result, models or measurements that describe properties without accounting for sample heterogeneity are up to now incomplete. For example, photoemission spectroscopy, energy dispersive spectroscopy, and inductively-coupled

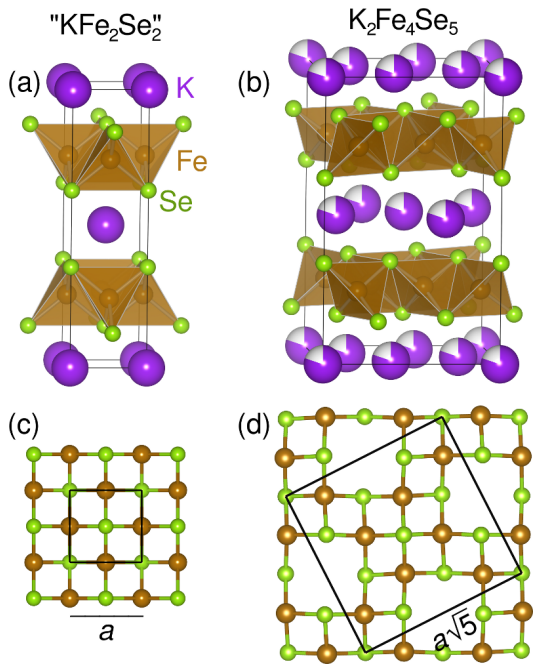

FIG. 1. (Color online) Unit cells for (a) hypothetical $I4/mmm$ fully-occupied KFe_2Se_2 and (b) Fe-vacancy ordered $K_2Fe_4Se_5$ which is equivalent to $K_{0.8}Fe_{1.6}Se_2$. Fe/Se nets are viewed down the c direction in (c) and (d).

plasma spectroscopy can only probe the composition of large portions of the samples–for a heterogeneous sample they do not describe any single component. Resolving multiple phases simultaneously is key in these systems, where a second metallic phase apart from pure $K_2Fe_4Se_5$ is believed to lead to superconductivity on the basis of NMR, muon spin resonance, and scanning probe measurements.[18, 23–25]

In order to understand why some samples are superconducting and some are not, we have conducted a systematic investigation of many samples. We prepared pure $K_2Fe_4Se_5$ and verified its existence using high-resolution synchrotron x-ray diffraction. We prepared superconducting crystals and investigated the changes in the $K_xFe_{2-y}Se_2$ lattice, including the appearance of three distinct additional phases: the metallic $K_xFe_2Se_2$ phase that precipitates coherently with $K_2Fe_4Se_5$ upon cooling and is the cause of superconductivity, a PbClF-type phase that forms due to exposure to moist air, and the insulator $KFe_{1.6}Se_2$ with full K occupancy and disordered Fe vacancies. All of these phases must be understood and controlled in order to explain the properties and diffraction data. We also show that the anomalous resistivity behavior, previously thought to signify a metal-insulator transition, [26] in fact arises from simple percolation of metallic and insulating phase fractions. With a more complete picture of the phase space in the $K_xFe_{2-y}Se_2$ system, we discuss implications for improved synthetic routes to superconducting intercalated iron selenides.

METHODS

Samples of $K_xFe_{2-y}Se_2$ were prepared from metallic K, Fe powder, and crushed Se shot (Alrich, 99.5%, 99.99%, and 99.99%, respectively). All manipulations were performed in a N_2-filled glovebox. Stoichiometric powders, including pure $K_2Fe_4Se_5$, were prepared by intimately mixing Fe and Se in a mortar and pestle in a N_2-filled glovebox with a ratio of 4Fe + 5Se, then loading in a carbon-coated quartz tube and sealing under vacuum. This tube was heated with a 12 h ramp to 700°C, 2 h hold, and furnace cool back to room temperature. This powder was ground again in a glovebox and loaded with K pieces in a covered alumina crucible in a quartz tube, sealed under vacuum, and heated over the same temperature profile. Finally, the powder was homogenized by grinding and fired with a 1 h ramp to 700°C, 10 h hold, and 1 h cool to room temperature.

Single crystals were prepared by prereaction of K pieces with Fe and Se powder in alumina crucibles sealed under vacuum and heated to 600 or 650°C in 12 h, with a 4 h hold and 4 h cool to room temperature, followed by grinding. Slow-cooled crystal growth was performed in alumina crucibles sealed under Ar in Nb tubes. Flame-melted samples were prepared by melting the prereacted powders in evcuated quartz tubes until the mixture was visibly molten. The nominal composition $K_xFe_{2-y}Se_2$ was varied from $0.8 \leq x \leq 0.85$ and $0 \leq y \leq 0.4$. Specific compositions and heat treatments are presented in the Supplemental Material.

High-resolution ($\Delta Q/Q < 2 \times 10^{-4}$) synchrotron powder diffraction data were collected using beamline 11-BM at the Advanced Photon Source (APS), Argonne National Laboratory using an average wavelength of 0.413 Å (∼30 keV). A NIST standard Si sample (SRM 640c) was used to calibrate the instrument, where the Si lattice constant determines the wavelength for each detector. Samples were sealed under vacuum in glass capillaries to prevent oxidation. Time-of-flight powder neutron diffraction measurements were conducted at the HIPD instrument at the Lujan Center, Los Alamos National Laboratory with samples sealed under He in vanadium cans. Rietveld refinements to synchrotron x-ray and neutron diffraction data were performed using GSAS.[27]

Laboratory x-ray powder diffraction was performed using a Philips X'Pert diffractometer with Cu-$K\alpha$ radiation, and Rietveld refinements were performed using the XND code.[28] Single-crystal diffraction data were collected on a STOE 2T image plate diffractometer with Mo-$K\alpha$ radiation ($\lambda = 0.71073$ Å) and X-Area software, and structures were refined using SHELXTL.[29] Four-probe resistivity, ac magnetic susceptibility, and heat capacity were measured using a Quantum Design PPMS.

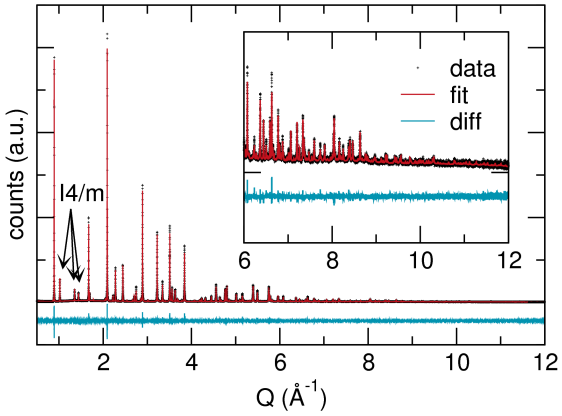

FIG. 2. (Color online) Rietveld refinement to high-resolution synchrotron diffraction data for powder $K_2Fe_4Se_5$ shows a pure compound with nearly complete vacancy ordering: only 7% of the Fe 4*d* sites are occupied. Low-angle peaks corresponding to the $I4/m$ cell due to Fe ordering are arrowed. High-Q data are enlarged in the inset to show fit quality. Structural details are given in Supplementary Information.

RESULTS AND DISCUSSION

Characterization of pure, polycrystalline $K_2Fe_4Se_5$

The composition-temperature phase space of $K_xFe_{2-y}Se_2$ is mostly unknown, so the need for a pure, homogeneous sample that can serve as a reference point is paramount. The most stable phase near superconductivity in this family is vacancy-ordered $K_2Fe_4Se_5$ with the unit cell shown in Figure 1. In this structure, first reported in $TlFe_{1.6}Se_2$,[30] the Fe vacancies order (lowering symmetry from $I4/mmm$ to $I4/m$) but the K vacancies are distributed randomly.[15] Single crystals of this compound can be grown from the melt, but high-temperature processing that involves melting results in samples that deviate from nominal stoichiometry

We developed a lower-temperature, solid-state route to form pure $K_2Fe_4Se_5$. The low-temperature procedure described in the experimental section consists of a pre-reaction of Fe and Se, followed by addition of K and multiple heatings to 700°C. To confirm phase purity we performed powder diffraction at APS beamline 11-BM, which provides exceptionally high-resolution data with high signal-to-noise ratio, while also maintaining capillary geometry that prevents air exposure. The Rietveld refinement shown in Figure 2 consists of sharp, unsplit peaks with no impurity phases, confirming the sample quality and homogeneity. At low angles the superstructure peaks from vacancy ordering are clearly visible, and arrowed in Figure 2. This sample refines to nearly complete vacancy ordering: only 7% of the Fe 4*d* sites are occupied. Detailed refinement results are given in the Supplemental Material.

This is a simple, reliable method for producing pure $K_2Fe_4Se_5$. Our magnetometry and resistivity measurements confirmed that $K_2Fe_4Se_5$ is an antiferromagnetic semiconductor.[15, 31, 32] While this powder synthesis provides great compositional control, we have never observed superconductivity in any powders created by this method, even when changing the stoichiometry in $K_xFe_{2-y}Se_2$ where $0.5 < x < 1$ and $1.4 < y < 2$.

This stoichiometric polycrystalline powder sample is crucial because it sets a structural reference point for which all other compositions will be compared. There is no evidence (line broadening, extra peaks, extra phases) in the 11-BM diffraction data for phase separation when pure $K_2Fe_4Se_5$ is made by this route.

Structural characterization of nominal $K_2Fe_4Se_5$ crystals

To date, there has been no mention of a superconducting powder of $K_xFe_{2-y}Se_2$, nor did we find one despite our efforts. This implies that melting and recrystallization may be required for the formation of the superconducting phase. We prepared single crystals of nominal $K_2Fe_4Se_5$ composition to determine how stoichiometry is affected by melting. Crystals prepared by melting nominal $K_2Fe_4Se_5$ formed plates which readily degrade in air, as judged by a change in color from shiny gold to matte brown.

Single crystal diffraction of these nominal $K_2Fe_4Se_5$ crystals shows superstructure Bragg peaks arising from $I4/m$ $K_2Fe_4Se_5$. These peaks form an octagon in the $(00l)$ reciprocal-space reconstruction in Figure 3, with the first peak at $(\frac{1}{5}\frac{3}{5}0)$ arrowed. Extra reflections appear at the (010) position of the $I4/mmm$ $K_{0.8}Fe_{1.6}Se_2$ lattice (arrowed in Figure 3) which is forbidden by I-centered symmetry. They do not represent a $\sqrt{2}\times\sqrt{2}$ modification of the $K_xFe_{2-y}Se_2$ structure, but instead arise from an oxidized phase that will be discussed in the next section. No other vacancy ordering patterns are observed in these crystals.

High-resolution x-ray diffraction was performed on ground batches of these crystals to search for phase separation in the form of split c-axis reflections, seen often in superconducting samples [14, 33, 34] and to screen for any minor impurities. Both are absent, and the fit from Rietveld refinement is shown in Figure 4.

We found that the lattice constants of nominal $K_2Fe_4Se_5$ crystals display an expanded a and contracted c-axis compared to the pure powder $K_2Fe_4Se_5$ (8.74536(8) × 14.10024(18) Å versus 8.721763(10) × 14.125178(23) Å for powder $K_2Fe_4Se_5$). The refined stoichiometry of the crystal was $K_{0.79(1)}Fe_{1.56(1)}Se_2$, while the ground batch of crystals had a refined composition of $K_{0.84(1)}Fe_{1.43(1)}Se_2$ from synchrotron powder diffraction. The difference between powder and single-crystal

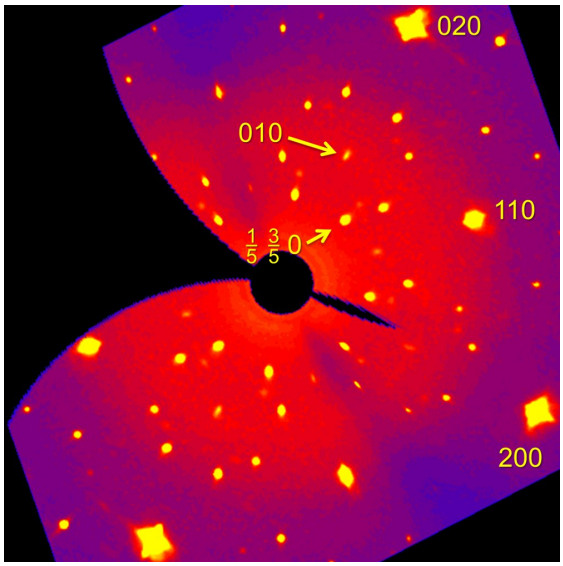

FIG. 3. (Color online) Reciprocal space reconstruction of single crystal x-ray diffraction data from a nominal $K_2Fe_4Se_5$ crystal. Reflections are labeled with Miller indices of the $I4/mmm$ $ThCr_2Si_2$ substructure. The fractional superstructure peaks, including the labeled peak at $(\frac{1}{5}\frac{3}{5}0)$, arise from vacancy ordering and lowering of symmetry to $I4/m$ The (010) reflection is forbidden by both I-centered cells, and represents a new, coherent phase. Subsequent analysis in this manuscript confirms it to be an oxidized phase with $c = 9$ Å.

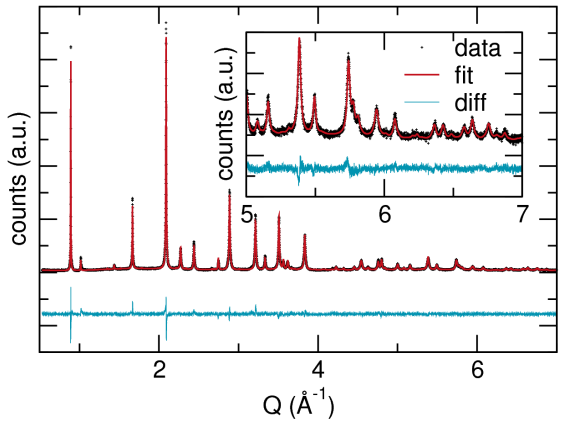

FIG. 4. (Color online) Rietveld refinement to high-resolution synchrotron diffraction data for a non-superconducting, ground single-crystal sample of nominal $K_2Fe_4Se_5$ composition. This sample displays $I4/m$ vacancy ordering.

measurements likely arises from heterogeneity among the crystals or systematic errors, but in any case both techniques find that $K_2Fe_4Se_5$ becomes Fe deficient after melting and recrystallization, and does not exhibit superconductivity. Still, the presence of an impurity phase in the single crystals merits further investigation, primarily to understand and avoid its conditions for formation.

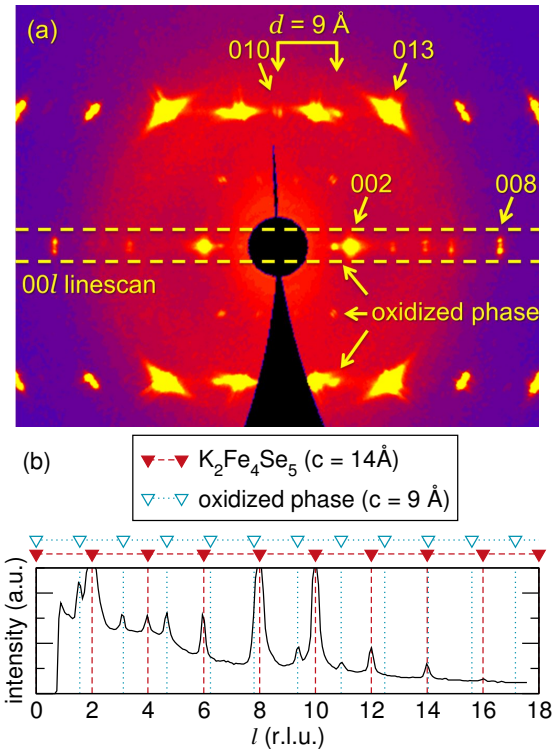

FIG. 5. (Color online) The reciprocal space reconstruction along the (100) direction of the parent $I4/mmm$ $K_{0.8}Fe_{1.6}Se_2$ lattice shows that the extra reflections, including (010) from Figure 3, lie along an l index that is distinct from $K_{0.8}Fe_{1.6}Se_2$. This distinct spacing is shown with $d = 9$ Å. An intensity linescan along 00l in (b) shows that these spots arise from a phase where the FeSe interlayer spacing is 9 Å, as opposed to $c/2 = 7$ Å for $K_2Fe_4Se_5$.

Forbidden (010) diffraction spots arise from the oxidized phase $K_{0.51(5)}Fe_{0.70(2)}Se$

The extra (010) Bragg reflections in the $K_{0.8}Fe_{1.6}Se_2$ reciprocal space reconstruction in Figure 3 merit further investigation to understand whether they might correspond to a $\sqrt{2} \times \sqrt{2}$ superstructure of the $K_xFe_{2-y}Se_2$ cell. Such a cell has been proposed on the basis of electron diffraction patterns viewed down the ⟨001⟩ direction. [35, 36] No such phase has ever been made in bulk quantities or detected by x-ray diffraction, and the electron diffraction peaks were not shown in the (0kl) or (h0l) directions to confirm registry with the $K_xFe_{2-y}Se_2$ lattice.

In Figure 5 we present the single crystal diffraction pattern from a perpendicular direction, down ⟨100⟩ in the (0kl) plane. From this vantage point the extra reflections form a vertical column with an l-spacing that is distinct from the major $K_{0.8}Fe_{1.6}Se_2$ peaks in the diffraction pattern. This column is at a distance $d = 9$ Å^{-1} from $l = 0$, arrowed in Figure 5(a). A line scan along the ⟨00l⟩ direction produced the intensity profile in Fig-

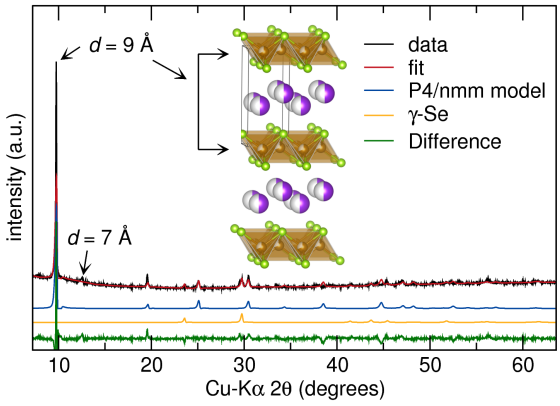

FIG. 6. (Color online) Powder XRD of the $K_2Fe_4Se_5$ after exposure to moist air shows conversion to the oxidized phase $K_{0.51(5)}Fe_{0.70(2)}Se$ with the PbClF structure, containing buckled K^+ layers and Fe vacancies. Results from single-crystal structure solution are given in the Supplemental Material.

TABLE I. Single-crystal refinement results for the oxidized phase $K_{0.51(5)}Fe_{0.698(19)}Se$. Space group: $P4/nmm$, a = 3.8952(6) Å, c = 9.1948(18)Å. Full refinement details are given in the Supplemental Material.

Atom	x	y	z	$U_{11} = U_{22}$	U_{33} (Å^2)	occupancy
K 2c	0.75	0.75	0.428(4)	0.140(10)	0.150(20)	0.51(5)
Fe 2a	0.75	0.25	0	0.045(3)	0.120(8)	0.698(19)
Se 2c	0.25	0.25	0.1559(6)	0.061(2)	0.116(4)	1

ure 5(b). The 00l reflections for the major $K_{0.8}Fe_{1.6}Se_2$ peaks are marked by dashed lines, while the minority phase is dotted. Assuming a tetragonal structure still built of FeSe tetrahedral layers, the smaller reciprocal-space repeat distance of the minor phase corresponds to an interlayer spacing of d = 9 Å.

In our case, this new phase is formed when crystals are screened and mounted for single crystal diffraction in paratone oil. Once the crystals are selected and placed in capillaries, the tubes are sealed and oxidation halts, resulting in only a minor fraction of this oxidized phase. If powder is exposed to moisture (dry oxygen does not react) for prolonged periods, full conversion to the oxidized phase occurs, as shown in the powder diffraction pattern in Figure 6. After full conversion to the new phase the supercell ordering disappears but the c = 9 Å Bragg peak remains. Only a tiny peak remains at $2\theta = 13°$, indicating almost full degradation of $K_xFe_{2-y}Se_2$. The new phase was determined from single-crystal diffraction to be a highly K- and Fe- deficient structure of the PbClF structure type, $K_{0.51(5)}Fe_{0.70(2)}Se$. This structure is common to a wide range of compounds, including the superconductor NaFeAs, which itself transforms to a $ThCr_2Si_2$ structure upon hydration.[37] Results from single-crystal refinement are shown in Table I, with full details given in the Supplemental Material. No superconducting behavior was seen in any samples after conversion to the oxidized phase.

Care must be taken to avoid air exposure of these samples, especially when surface-sensitive measurements are made. The expulsion of Se from the structure seen in Figure 6 implies that Fe^{2+} is being oxidized. This phase may explain why substantial c-axis disorder was seen in x-ray absorption measurements.[38] Abnormally small Fe–Fe distances were also seen in that study, which can be explained by the metallic superconducting minor phase which we address subsequently.

Formation of this rapidly forming oxidized phase may go unobserved in surface-sensitive measurements since it is coherent with the parent phase of $K_2Fe_4Se_5$ from which it originates. Therefore, any studies of these samples where a significant exposure to air has occurred during handling (several minutes) may be tainted by interference from the oxidized phase of $K_{0.51(5)}Fe_{0.70(2)}Se$. Presence of this oxidized phase and the superconducting minority phase, which we discuss subsequently, should be considered when interpreting angle-resolved photoemission spectroscopy in particular, where a $\sqrt{5} \times \sqrt{5}$ supercell is not seen.[39]

Superconducting $K_xFe_{2-y}Se_2$: Changes in the $I4/m$ majority phase and evidence for phase separation

We grew superconducting crystals using the same procedure as our nominal $K_2Fe_4Se_5$ crystals, except the nominal stoichiometry was $K_{0.85}Fe_{1.9}Se_2$. These crystals appear visually similar, but excess iron precipitates as metal and often pervades the solidified ingot, with its highest concentration at the top of the ingot. Iron is denser than $K_2Fe_4Se_5$ (7.8 versus 4.3 g/cc) so it was most likely pushed upward by the advancing solidification front and not floating on the selenide melt. The extent of Fe solubility in $K_xFe_{2-y}Se_2$ melts remains unknown, and may be a key in determining how to control phase separation in these materials.

Reciprocal-space reconstructions of a superconducting crystal from single-crystal x-ray diffraction (Figure 7) show the supercell reflections from vacancy-ordered $K_2Fe_4Se_5$. The single-crystal refined composition is $K_{0.72(2)}Fe_{1.63(1)}Se_2$, but the question of phase separation is crucially important, since a distinct phase that induces superconductivity may be present. [40–43] Our laboratory single-crystal diffractometer could not resolve any new reflections that were not present in nominal, non-superconducting $K_2Fe_4Se_5$ crystals, so we performed high-resolution synchrotron powder diffraction to investigate the totality of phases present in these materials.

A comparison of the Bragg peak splitting in superconducting crystals (nominal $K_{0.85}Fe_{1.9}Se_2$) and non-superconducting samples (nominal $K_2Fe_4Se_5$ crystals and powder) is shown in Figure 8. The superconduct-

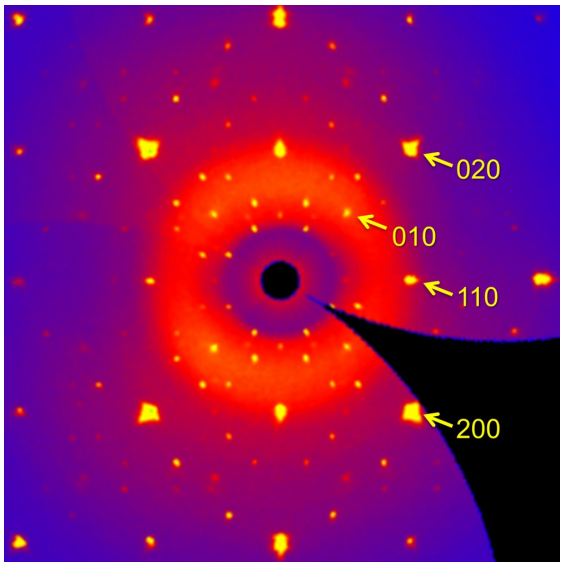

FIG. 7. (Color online) Reciprocal-space reconstruction of a superconducting crystal of nominal $K_{0.85}Fe_{1.9}Se_2$ composition, with the octagon of twinned peaks corresponding to $K_2Fe_4Se_5$. Reflections are labeled with Miller indices of the $I4/mmm$ substructure. Again, the (110) peak is present due to formation of the oxidized phase after minor air exposure.

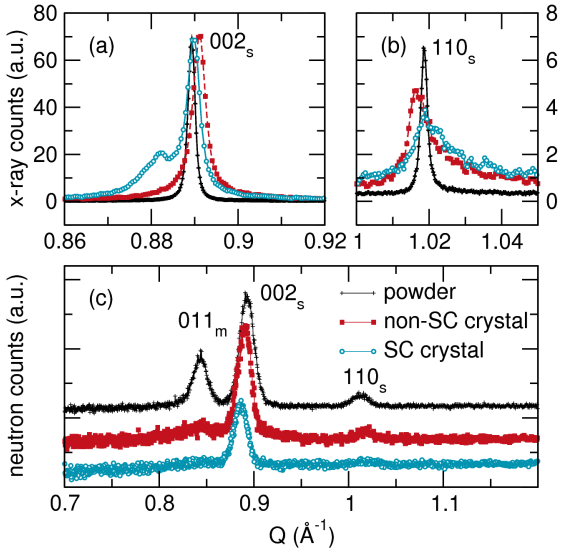

FIG. 8. (Color online) Comparison of diffraction peaks for powder $K_2Fe_4Se_5$ versus non-superconducting crystals (nominal $K_2Fe_4Se_5$) and superconducting crystals (nominal $K_{0.85}Fe_{1.9}Se_2$). All data were collected at 300 K. In (a), the synchrotron diffraction peak (002) shows a split of the c-axis in the SC sample. In (b), the magnified (110) peak shows significant disorder in the *ab* plane in both crystals. In (c), the magnetic (011) reflection viewed by neutron diffraction from HIPD shows strong magnetic ordering in the powder, weak magnetic ordering in nominal $K_2Fe_4Se_5$ crystals, and no magnetic ordering in superconducting nominal $K_{0.85}Fe_{1.9}Se_2$.

ing crystals display a clear split of the (002) reflection. This splitting is commonly seen when Rb, Cs, and K-containing single crystals are characterized using simple Bragg-Brentano diffraction measurements, [33, 34] and most likely represents the metallic superconducting phase which we discuss in the next section. There is no splitting in Figure 8(a) for the non-superconducting nominal $K_2Fe_4Se_5$ crystal or powder. This implies that phase separation is not an intrinsic feature of pure $K_2Fe_4Se_5$. Rather, deviations from that stoichiometry are required to drive phase separation. The (110) peak of the $I4/m$ vacancy-ordered phase is compared in Figure 8(b), and both single crystalline samples are considerably broadened, with a long tail on the high-Q side of the peak, in the direction of β-FeSe which has its (110) peak at $Q = 1.17$ Å^{-1}.

Stoichiometric deviation from pure $K_2Fe_4Se_5$ leads to weakening of antiferromagnetic order. Neutron powder diffraction at 300 K in Figure 8(c) shows a strong (011) magnetic peak at $Q = 0.84$ Å^{-1}, indicating strong antiferromagnetic order in pure powder $K_2Fe_4Se_5$, which has $T_N = 559$°C.[44] This peak is substantially weakened in the nominal $K_2Fe_4Se_5$ crystal, and has disappeared in the superconducting crystal. Indeed, subtle changes in stoichiometry disrupt the magnetic ordering in the $K_xFe_{2-y}Se_2$ lattice, and antiferromagnetism and superconductivity appear mutually exclusive.

The superconducting metallic phase $K_xFe_2Se_2$

The 11-BM synchrotron x-ray data resolves splitting in not only the the (002) reflection, but an entirely separate $I4/mmm$ phase that occurs in superconducting samples, shown in the insets of Figure 9(a,b,c). These extra peaks can be modeled using a separate cell with disordered vacancies. For three separate superconducting samples, this phase refines to a composition of $K_xFe_2Se_2$ where $x = 0.38(2)$, $0.55(1)$, and $0.58(2)$, with weight fractions of 13, 18, and 12%. Rietveld refinement results are summarized in Table II. Full details are given in the Supplemental Material. Our compositions, along with those determined by a lower-resolution diffraction study,[42] and NMR measurements [23] all find evidence for the metallic minority phase to have nearly full iron occupancy and K deficiency. This phase must not display any K^+ vacancy ordering, as any superstructure peaks arising from ∼15% of the sample would be clearly visible in the single-crystal diffraction pattern (Figure 7). Recent high-temperature diffraction data have confirmed that this phase is absorbed into $K_2Fe_4Se_5$ above the vacancy ordering temperature.[43]

All three samples which exhibited phase separated $K_xFe_2Se_2$ (3, 4, and 6 in Figure 10) by synchrotron diffraction displayed a diamagnetic response at T_c. No semiconducting samples contained this minority

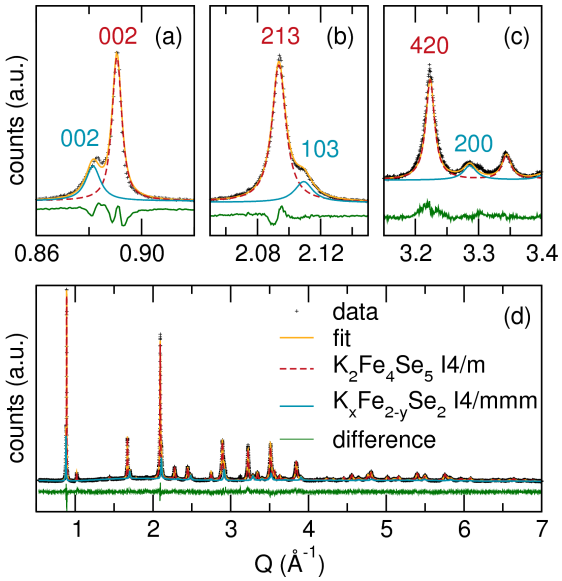

FIG. 9. (Color online) Rietveld refinement to high-resolution synchrotron x-ray diffraction data of a superconducting sample of nominal $K_{0.85}Fe_{1.9}Se_2$ composition displays peak splitting corresponding to a distinct $I4/mmm$ phase at room temperature. Selected regions are expanded in (a,b,c) to show detail on equivalent pairs of reflections. The labeled peaks would be coincident for both phases in the absence of lattice distortions.

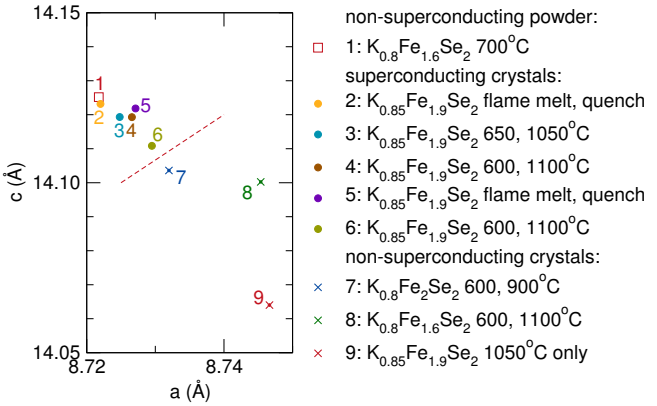

FIG. 10. (Color online) Lattice parameters for the bulk $K_xFe_{2-y}Se_2$ phase with $I4/m$ structure obtained from Rietveld refinement of high-resolution synchrotron diffraction data display a narrow range of c-axis for superconducting samples, but only in crystals grown from the melt. Temperatures of pre-reaction and subsequent crystal growth are shown for each sample. Refined parameters and detailed synthesis conditions are given in the Supplemental Material.

TABLE II. Rietveld refinement results for the superconducting metallic phase $K_xFe_2Se_2$ for three different samples. Sample numbers correspond to points in Figure 10 and to the full refinement details and processing conditions given in the Supplemental Material.

#		Stoichiometry	wt%	a (Å)	c (Å)
3	R_{wp}	$K_{0.58(2)}Fe_{1.84(4)}Se_2$	12	3.83414(20)	14.2360(12)
4	R_{wp}	$K_{0.55(1)}Fe_{2.00(2)}Se_2$	18	3.82803(23)	14.2634(10)
6	R_{wp}	$K_{0.38(2)}Fe_{2.06(28)}Se_2$	13	3.82707(26)	14.2658(15)

$I4/mmm$ phase. Two samples, (2 and 5 in Figure 10) were superconducting but the diffraction peaks were too broad to resolve the second phase due to quenching. While samples with a small superconducting fraction can be made reliably, creating homogeneous samples is a requirement for understanding the mechanisms of superconductivity in these samples, for example by photoemission spectroscopy or inelastic neutron scattering. To that end, we have begun to map the available phases in the $K_xFe_{2-y}Se_2$ system and probe their stability.

The previous claim that KFe_2Se_2 is the superconducting phase seems implausible since this formula requires half to the Fe atoms to be in the 1+ state and tetrahedrally coordinated by Se. Such a state is unlikely to be stable since it requires excessive negative charge on a large fraction of the Fe atoms and is unprecedented in the literature. On the other hand, a $K_xFe_2Se_2$ formulation with $x \sim 0.5$ would require only a quarter of Fe atoms to be in a 1+ state and in this case the extra negative charge may be delocalized over a broad conduction band.

Changes in $I4/m$ structure of $K_2Fe_4Se_5$ seen by Rietveld refinement

In all our samples, regardless of superconductivity, the $I4/m$ $K_2Fe_4Se_5$ phase is present. We have searched via Rietveld refinement for systematic changes in the $I4/m$ phase that might be associated with the onset of superconductivity.

Lattice parameters for the $I4/m$ phase are given in Figure 10. Sample 1 is a pure powder (non-superconducting) of $K_2Fe_4Se_5$. The cluster of superconducting samples all have an a-axis smaller than 8.73 Å and a c-axis larger than 14.11 Å, distinct from the non-superconducting crystals and separated by a dashed line. However these lattice parameters are not a structural trigger of superconductivity, since the insulating powder sample falls in the superconducting range. Instead we assert that the superconducting samples contain a majority $I4/m$ component that is near the edge of its compositional range, and so are predisposed to containing the minority $K_xFe_2Se_2$ superconducting phase.

The stoichiometries of all $I4/m$ $K_xFe_{2-y}Se_2$ phases from Rietveld refinements are shown in Figure 11(a). The superconducting samples are tightly clustered in composition space, but there is no distinction between them and the non-superconducting samples. K contents are near nominal values, while Fe tends to be deficient, around $K_xFe_{1.5}Se_2$. An approximate calculation of Fe valence us-

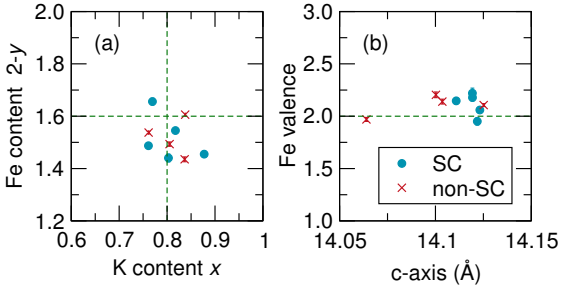

FIG. 11. (Color online) K and Fe content from Rietveld refinements of the majority $I4/m$ phases in superconducting (SC) and non-superconducting samples show no clear distinction between the two groups. Fe tends to be slightly deficient in superconducting samples. Fe valence derived from Rietveld-refined stoichiometry shows a strong tendency for majority Fe^{2+} in the $I4/m$ phase.

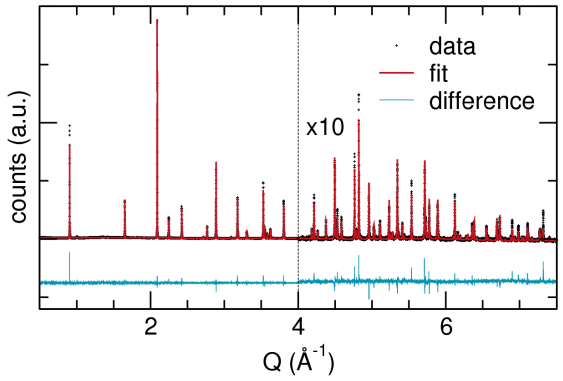

FIG. 12. (Color online) Synchrotron x-ray diffraction Rietveld refinement of a vacancy-disordered, non-superconducting $K_{0.959(4)}Fe_{1.606(6)}Se_2$ powder sample with fully-occupied K sites. Refinement results are given in the Supplemental Material.

ing these refined stoichiometries is shown in Figure 11(b). The non-superconducting and superconducting samples are both clustered around Fe^{2+}.

A clear division was seen in lattice parameters (Figure 10) for superconducting and non-superconducting samples, but not in the refined stoichiometry (Figure 11). As a result, the lattice parameters may be a more exact probe of the response of the $K_2Fe_4Se_5$-type $I4/m$ lattice to stoichiometry, and further work should be done to explain how the lattice parameters change with K and Fe content, and their relation to phase separation, which is now believed to be necessary for superconductivity. [18–20] We present preliminary work on this subject in the next section.

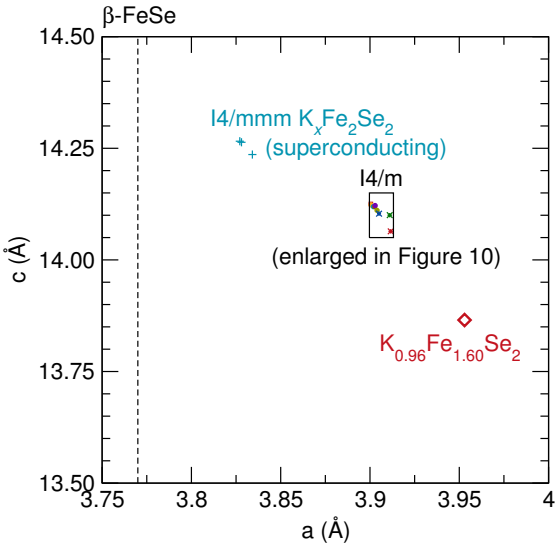

FIG. 13. (Color online) Trends of a and c lattice parameters at 300 K across the $K_xFe_{2-y}Se_2$ phase space, as determined by Rietveld refinement to high-resolution synchrotron diffraction data. The trend implies that the minority phase in superconducting samples is very K-deficient, and distinct from the stability regions of pure β-FeSe or $I4/m$ $K_2Fe_4Se_5$.

Comparing related phases in the $K_xFe_{2-y}Se_2$ series: β-FeSe, $K_xFe_2Se_2$, $K_2Fe_4Se_5$, and $KFe_{1.6}Se_2$

Hypothetically, the $K_xFe_{2-y}Se_2$ phase space could contain a plethora of homologous $(K_2Se)(FeSe)_n$ phases containing strictly Fe^{2+}, from $n = 3$ $K_2Fe_3Se_4$, where the K layer is filled, to $n = \infty$ corresponding to β-FeSe. Our attempts to produce phases with higher n ($K_2Fe_5Se_6$, $K_2Fe_6Se_7$, etc.) by solid state reactions simply led to $K_2Fe_4Se_5$ + β-FeSe. Reactions with the nominal composition $K_2Fe_3Se_4$ gave a pure compound, and upon synchrotron x-ray diffraction the refined occupancy was found to be $K_{0.959(4)}Fe_{1.606(6)}Se_2$, with excess K and Se likely precipitating as amorphous K_2Se_4.[45] There are no superstructure peaks in this compound, indicating that the Fe vacancies are truly disordered and the symmetry remains $I4/mmm$. The fit from Rietveld refinement is shown in Figure 12, and results are tabulated in the Supplemental Material. The isostructural phase $TlFe_{1.6}Se_2$ exhibits multiple magnetic transitions at low temperatures, [46, 47] so further investigation is warranted. We did not detect any superconducting diamagnetic response in $KFe_{1.6}Se_2$ down to 2 K.

The $KFe_{1.6}Se_2$ phase represents a third distinct phase in the $K_xFe_{2-y}Se_2$ system, in addition to $K_2Fe_4Se_5$ and $K_xFe_2Se_2$. The lattice parameters of all these phases are shown in Figure 13, (with the $I4/m$ phase normalized by $\sqrt{5}$). This diagram provides a full view of known phases in the $K_xFe_{2-y}Se_2$ system, from full K occupancy in $KFe_{1.6}Se_2$ to empty interlayer space in β-FeSe. A trend of decreasing a with increasing c is evident, likely driven by

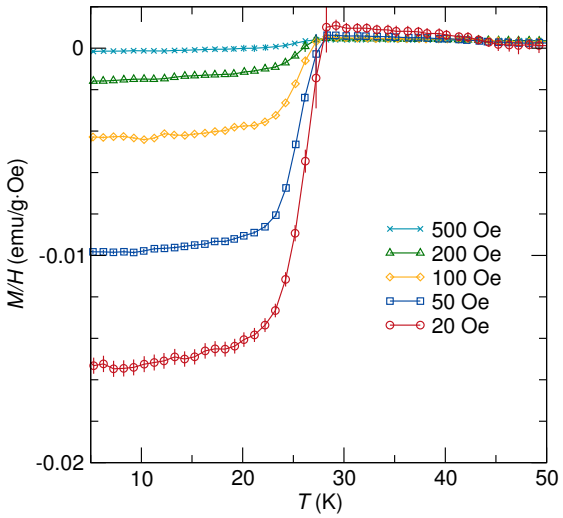

FIG. 14. (Color online) Magnetization of a superconducting sample of nominal $K_{0.85}Fe_{1.9}Se_2$ composition.

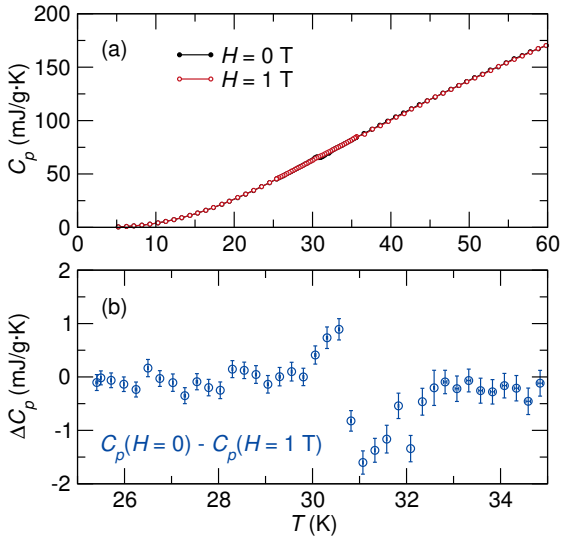

FIG. 15. (Color online) Heat capacity of a superconducting crystal shows a very small anomaly at T_c. This feature is magnified in (b) by subtracting the $H = 1$ T measurement from the zero-field measurement.

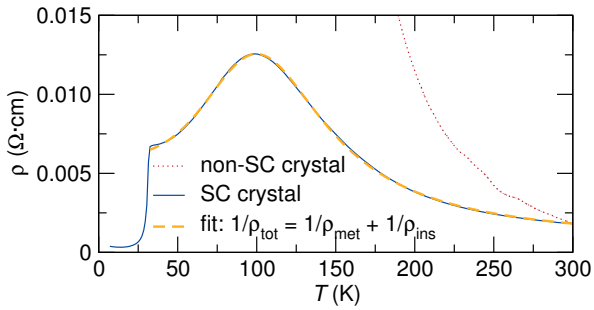

FIG. 16. (Color online) Resistivity of non-superconducting $K_2Fe_4Se_5$ crystal and a nominal $K_{0.85}Fe_{1.9}Se_2$ superconducting crystal. The $K_2Fe_4Se_5$ is an insulator, but the superconductor behavior can be fit as a metallic and insulating composite over the full temperature range.

weak van der Waals interlayer forces yielding to stronger ionic bonding as K^+ is inserted. Simultaneous carrier donation from K^+ into the FeSe layers leads to weaker Fe-Se bonding and an increase in intralayer distances (a lattice parameters). From this plot, the separation between $I4/m$ $K_2Fe_4Se_5$ phases and the superconducting minority phases is shown to be quite significant. We discuss implications for the synthesis of this phase subsequently. It remains to be seen if there is a solid solution between $K_2Fe_4Se_5$ and $KFe_{1.6}Se_2$.

Superconducting composite of $K_2Fe_4Se_5$ and $K_xFe_2Se_2$: Magnetometry and heat capacity

DC magnetometry of a superconducting sample (sample 6) is shown in Figure 14, with $T_c = 28$ K. Such measurements are unfortunately not a viable way to probe the superconducting volume fraction. If the fraction is small but pervades the entire sample, as in a net-like model,[48] then magnetometry would give an inflated view of the volume fraction. For this reason, we performed heat capacity measurements on samples that had already been confirmed to be superconducting by magnetometry.

Heat capacity measurements provide an excellent way to confirm bulk superconductivity, although the precise volume fraction would depend on a known model for the entropy release at T_c. Studies on $YBa_2Cu_3O_{7-\delta}$ and β-FeSe have shown clear signatures of entropy release ($\Delta C_p \approx 6.9$ and 3 mJ/gK, respectively) across T_c. [9, 49] We measured a single crystal (sample 6) with a strong zoom across T_c and the measurement is seen in Figure 15. The inset in Figure 15(b) shows the difference between heat capacity measured at zero field and $H = 1$ T. The anomaly at $T = 31$ K is approximately 2 mJ/gK, which is comparable to β-FeSe, even though the fraction of $K_xFe_2Se_2$ phase is only ~15% by weight. The small peak in this data confirms the minor phase fraction of superconducting $K_xFe_2Se_2$ seen in powder diffraction patterns and magnetic susceptibility. Further evidence for this two-phase coexistence is seen in resistivity measurements.

Resistivity: Metal-insulator crossover implies two-phase coexistence

Resistivity (ρ) measurements from superconducting and non-superconducting crystals are shown in Figure 16. The ρ drops to zero at $T_c = 31$ K, in agreement with our magnetization and heat capacity measurements.

There is a hump in the resistivity around 100 K, which was seen in many studies, including the initial report by Guo, et al [2, 10, 50] and attributed to a metal-insulator transition.[26] However, given the phase separation between $K_2Fe_4Se_5$ and $K_xFe_2Se_2$, it is more likely that the metallic and insulating phases are *always* present. Thus the full resistivity range can be fit using a model of two percolating phases that act as resistors in parallel, one with metallic Bloch-Grüneisen temperature dependence ρ_{metal} and the other with Boltzmann-type insulating temperature dependence ρ_{ins}:

$$1/\rho_{total} = 1/\rho_{metal} + 1/\rho_{semi} \quad (1)$$

$$\rho_{metal}(T) = \rho(0) + AT^n \quad (2)$$

$$\rho_{semi}(T) = \rho_0 e^{\frac{E_g}{2kT}} \quad (3)$$

Where $\rho(0)$, A, and ρ_0 are all constants that depend on phase fractions and geometry in this case. This fit (dashed in Figure 16) is excellent and gives $n = 2.78$, and insulator activation energy of $E_g = 83$ meV. Changes in the position of the hump can be accomplished by simply changing the relative volume fractions of these two phases. The metallic phase is not iron since it is present in such small amounts ($\leq 2\%$ by weight by synchrotron powder diffraction). Furthermore, muon spin rotation and scanning probe measurements indicate that the superconducting phase is metallic above T_c. [18, 24, 51] This resistivity maximum provides further confirmation that the minority $I4/mmm$ phase is the cause of superconductivity, and further work should be conducted to optimize its synthesis.

Implications for synthesis

Pure, bulk superconducting samples of $K_xFe_{2-y}Se_2$ remain elusive, but careful structural studies can explain why this phase is difficult to synthesize. First, it is surprising that $K_xFe_2Se_2$ forms from solid state reactions because all known alkali iron chalcogenides have Fe valence nearly 2+ or 3+. We attempted to intercalate K into β-FeSe by vapor transport in a sealed tube at 300°C. However this reaction only resulted in the formation of K_2Se and metallic Fe, and no increase in T_c above 8 K. Why then does Fe-rich phase $K_xFe_2Se_2$ form during heat treatment of $K_xFe_{2-y}Se_2$?

We propose that the metallic superconducting fraction precipitates upon cooling through the Fe vacancy ordering temperature at ∼540 K,[43] but only in cases where the crystal size is large enough for lattice strain to prevent escape of supersaturated Fe from the $K_xFe_{2-y}Se_2$ structure. Formation of a coherent intergrowth of this $I4/mmm$ phase is supported by recent evidence from electron microscopy and muon spin rotation.[17, 24] We have not observed superconductivity in polycrystalline powder samples, indicating lattice strain may be a key factor. If T_c is eventually observed in powders, it would mean that the Fe supersaturation in the $K_xFe_{2-y}Se_2$ structure at high temperatures is the only prerequisite for formation of $K_xFe_2Se_2$.

Only a small amount of Fe excess can be incorporated in the $K_xFe_{2-y}Se_2$ structure at high temperatures. This places a limit on the volume of minority $I4/mmm$ phase that will precipitate when cooling through the vacancy ordering temperature. The separation between the maximum Fe solubility at high temperatures and 80% Fe occupancy (in $K_2Fe_4Se_5$) determines the amount of $K_xFe_2Se_2$ that can form. This explains why superconducting samples show $I4/m$ lattice parameters on the edge of the $K_2Fe_4Se_5$ stability region in Figure 10, and why the heat capacity measurements and powder diffraction both find a small volume fraction of superconducting phase.

Solid-state routes toward single-phase, superconducting $K_xFe_2Se_2$ will require an understanding of, and control over, the delicate temperature-composition space in the region between $K_2Fe_4Se_5$ and β-FeSe. In-situ experiments (diffraction, calorimetry, or vibrational spectroscopy) that investigate the limit of Fe solubility in $K_xFe_{2-y}Se_2$ around and above the vacancy ordering temperature may prove invaluable. Quenching from above this temperature has shown to increase the sharpness of the superconducting transition, [13, 14] and understanding the kinetics of this transition may provide insight into stabilizing Fe-rich phases. Topotactic reactions at low temperatures, such as those conducted in liquid ammonia, seem to have the ability to intercalate β-FeSe without significant expulsion of Fe, [52–54] while oxidative deintercalation as was performed on KNi_2Se_2 may approach $K_xFe_2Se_2$ by removal of K^+.[55]

Expanding the available $I4/mmm$ composition space by doping may provide new routes to stabilize phases similar to $K_xFe_2Se_2$. The response of $ThCr_2Si_2$ structures with substitution of Se^{2-} for As^{3-} has not been systematically investigated. Only the solid solution $K_xFe_{2-y}(Se,S)_2$ has been investigated (albeit without a description of subtle phase separation). [26] Even simple phase equilibria studies, such as the evolution of phases across nominal $K_xFe_2Se_2$ ($0 \leq x \leq 1$) from room temperature to ∼1250 K remain unknown.

CONCLUSIONS

The stable phase close to superconducting stoichiometry, vacancy-ordered $K_2Fe_4Se_5$ phase can be made pure by a solid state powder reaction. We find no evidence that this $I4/m$ phase can be doped or substituted to become superconducting. As a result, high-resolution

diffraction experiments are needed to detect the presence of additional phases.

The metallic minority phase $K_xFe_2Se_2$ with $I4/mmm$ symmetry appears only in samples that exhibit superconductivity, as judged by a diamagnetic response around $T_c = 30$ K. This phase does not exhibit any vacancy ordering. It only occurs in large crystals of $K_xFe_{2-y}Se_2$ grown from the melt, so the excess Fe is likely trapped by lattice strain, forming a coherent intergrowth with a volume fraction that is limited by the solubility of excess Fe above the vacancy ordering temperature of $K_2Fe_4Se_5$. This model of phase separation is supported by our resistivity measurements, which indicate a percolative composite of an insulator and metal, which is supported by local NMR and muon spin resonance probes and electron microscopy studies. [18, 23, 24, 43]

We identified an oxidized phase $K_{0.51(5)}Fe_{0.70(2)}Se$ as the cause of (010) reflections in the single-crystal diffraction pattern that are forbidden by I-centered symmetry. This phase has a FeSe interlayer spacing of 9 Å, which is highly expanded versus the 7 Å spacing of $K_2Fe_4Se_5$, due to buckling of the K layer after oxidation of Fe and loss of Se. This phase forms in the PbClF structure, similar to NaFeAs. It is not relevant to superconducting behavior, and sufficient care must be taken to prevent exposure of $K_xFe_{2-y}Se_2$ samples to moisture.

Yet another phase, $KFe_{1.6}Se_2$ was identified to form with disordered vacancies ($I4/mmm$) and pure polycrystalline powders were obtained by solid state reaction. This phase was produced when we attempted to synthesize the hypothetical ordered compound $K_2Fe_3Se_4$ in the homologous series $(K_2Se)(FeSe)_n$. The response of the $K_xFe_{2-y}Se_2$ lattice as stoichiometry is varied from $KFe_{1.6}Se_2$ to $K_2Fe_4Se_5$, $K_xFe_2Se_2$, and β-FeSe may prove to be a valuable probe of phase equilibria and electrical response in these systems, especially because the Rietveld-refined K/Fe stoichiometry does not provide a definitive picture of the divide between superconducting and non-superconducting samples.

Further investigations of superconducting $K_xFe_2Se_2$ must embrace the fact that these phases are unstable and heterogeneous. More informed synthesis should be pursued by investigating the high-temperature phase relations in these systems, and by understanding the kinetic processes occurring when the superconducting minority phase separates from related $K_2Fe_4Se_5$.

Finally, the insights obtained from this work call for detailed transmission electron microscopy studies to understand the superconducting/semiconducting interface and assess the nature of strain and defects associated with it. Clearly, bulk phase separation can form such composite structures. Phase separation can proceed by nucleation and growth or spinodal decomposition. The dividing line between them depends crtically on the strain that develops in the system during phase separation. According to our studies, $K_2Fe_4Se_5$ and $K_xFe_2Se_2$ have a lattice mismatch of 1-2%, leading to considerable strains. Our present results call for first principles studies of the thermodynamics of incoherent and coherent phase separation in the $K_2Fe_4Se_5/K_xFe_2Se_2$ systems to calculate strain energies and mixing energies.

ACKNOWLEDGMENTS

Work at Argonne National Laboratory is supported by UChicago Argonne, a U.S. DOE Office of Science Laboratory, operated under Contract No. DE-AC02-06CH11357. This work utilized the HIPD instrument at the Los Alamos Neutron Science Center, funded by the DOE Ofce of Basic Energy Sciences and operated by Los Alamos National Security LLC under Contract No. DE-AC52-06NA25396.

* m-kanatzidis@northwestern.edu

[1] F.-C. Hsu, J.-Y. Luo, K.-W. Yeh, T.-K. Chen, T.-W. Huang, P. M. Wu, Y.-C. Lee, Y.-L. Huang, Y.-Y. Chu, D.-C. Yan, and M.-K. Wu, Proc. Nat. Acad. Sci. **105**, 14262 (2008).
[2] J. Guo, S. Jin, G. Wang, S. Wang, K. Zhu, T. Zhou, M. He, and X. Chen, Phys. Rev. B **82**, 180520 (2010).
[3] F. Ye, S. Chi, W. Bao, X. F. Wang, J. J. Ying, X. H. Chen, H. D. Wang, C. H. Dong, and M. Fang, Phys. Rev. Lett. **107**, 137003 (2011).
[4] J. Wen, G. Xu, G. Gu, J. M. Tranquada, and R. J. Birgeneau, Rep. Prog. Phys. **74**, 124503 (2011).
[5] A. Ivanovskii, Physica C **471**, 409 (2011).
[6] D.-x. Mou, L. Zhao, and X.-j. Zhou, Front. Phys. **6**, 410 (2011).
[7] K. Syu, H. Sung, and W. Lee, Physica C **471**, 591 (2011).
[8] S. Avci, O. Chmaissem, D. Y. Chung, S. Rosenkranz, E. A. Goremychkin, J. P. Castellan, I. S. Todorov, J. A. Schlueter, H. Claus, A. Daoud-Aladine, D. D. Khalyavin, M. G. Kanatzidis, and R. Osborn, Phys. Rev. B **85**, 184507 (2012).
[9] T. M. McQueen, Q. Huang, V. Ksenofontov, C. Felser, Q. Xu, H. Zandbergen, Y. S. Hor, J. Allred, A. J. Williams, D. Qu, J. Checkelsky, N. P. Ong, and R. J. Cava, Phys. Rev. B **79**, 014522 (2009).
[10] Y. J. Yan, M. Zhang, A. F. Wang, J. J. Ying, Z. Y. Li, W. Qin, X. G. Luo, J. Q. Li, J. Hu, and X. H. Chen, Sci. Rep. **2** (2012).
[11] M.-H. Fang, H.-D. Wang, C.-H. Dong, Z.-J. Li, C.-M. Feng, J. Chen, and H. Q. Yuan, Europhys. Lett. **94**, 27009 (2011).
[12] W. Bao, G. N. Li, Q. Huang, G. F. Chen, J. B. He, M. A. Green, Y. Qiu, D. M. Wang, and J. L. Luo, arXiv:1102.3674 (2011).
[13] F. Han, H. Yang, B. Shen, Z.-Y. Wang, C.-H. Li, and H.-H. Wen, Phil. Mag. **92**, 2553 (2012).
[14] T. Ozaki, H. Takeya, H. Okazaki, K. Deguchi, S. Demura, Y. Kawasaki, H. Hara, T. Watanabe, T. Yamaguchi, and Y. Takano, Europhys. Lett. **98**, 27002 (2012).

[15] J. Bacsa, A. Y. Ganin, Y. Takabayashi, K. E. Christensen, K. Prassides, M. J. Rosseinsky, and J. B. Claridge, Chem. Sci. **2**, 1054 (2011).

[16] W. Bronger, A. Kyas, and P. Mller, J. Solid State Chem. **70**, 262 (1987).

[17] D. H. Ryan, W. N. Rowan-Weetaluktuk, J. M. Cadogan, R. Hu, W. E. Straszheim, S. L. Budko, and P. C. Canfield, Phys. Rev. B **83**, 104526 (2011).

[18] D. A. Torchetti, M. Fu, D. C. Christensen, K. J. Nelson, T. Imai, H. C. Lei, and C. Petrovic, Phys. Rev. B **83**, 104508 (2011).

[19] V. Ksenofontov, G. Wortmann, S. A. Medvedev, V. Tsurkan, J. Deisenhofer, A. Loidl, and C. Felser, Phys. Rev. B **84**, 180508 (2011).

[20] L. Ma, G. F. Ji, J. Dai, J. B. He, D. M. Wang, G. F. Chen, B. Normand, and W. Yu, Phys. Rev. B **84**, 220505 (2011).

[21] X.-W. Yan, M. Gao, Z.-Y. Lu, and T. Xiang, Phys. Rev. B **83**, 233205 (2011).

[22] W. Lv, W.-C. Lee, and P. Phillips, Phys. Rev. B **84**, 155107 (2011).

[23] Y. Texier, J. Deisenhofer, V. Tsurkan, A. Loidl, D. S. Inosov, G. Friemel, and J. Bobroff, Phys. Rev. Lett. **108**, 237002 (2012).

[24] A. Charnukha, A. Cvitkovic, T. Prokscha, D. Pröpper, N. Ocelic, A. Suter, Z. Salman, E. Morenzoni, J. Deisenhofer, V. Tsurkan, A. Loidl, B. Keimer, and A. V. Boris, Phys. Rev. Lett. **109**, 017003 (2012).

[25] F. Chen, M. Xu, Q. Q. Ge, Y. Zhang, Z. R. Ye, L. X. Yang, J. Jiang, B. P. Xie, R. C. Che, M. Zhang, A. F. Wang, X. H. Chen, D. W. Shen, J. P. Hu, and D. L. Feng, Phys. Rev. X **1**, 021020 (2011).

[26] H. Lei, M. Abeykoon, E. S. Bozin, K. Wang, J. B. Warren, and C. Petrovic, Phys. Rev. Lett. **107**, 137002 (2011).

[27] A. Larson and R. Von Dreele, Los Alamos National Laboratory Report LAUR **86**, 748 (2000).

[28] J. Bérar and G. Baldinozzi, IUCr-CPD Newsletter **20**, 3 (1998).

[29] G. M. Sheldrick, Acta Cryst. A **64**, 112 (2007).

[30] L. Häggström, H. Verma, S. Bjarman, R. Wäppling, and R. Berger, J. Solid State Chem. **63**, 401 (1986).

[31] Y. J. Song, Z. Wang, Z. Wang, H. L. Shi, Z. Chen, H. F. Tian, G. F. Chen, H. X. Yang, and J. Q. Li, Europhys. Lett. **95**, 37007 (2011).

[32] V. Svitlyk, D. Chernyshov, E. Pomjakushina, A. Krzton-Maziopa, K. Conder, V. Pomjakushin, and V. Dmitriev, Inorg. Chem **50**, 10703 (2011).

[33] X. G. Luo, X. F. Wang, J. J. Ying, Y. J. Yan, Z. Y. Li, M. Zhang, A. F. Wang, P. Cheng, Z. J. Xiang, G. J. Ye, R. H. Liu, and X. H. Chen, New Journal of Physics **13**, 053011 (2011).

[34] H.-D. Wang, C.-H. Dong, Z.-J. Li, Q.-H. Mao, S.-S. Zhu, C.-M. Feng, H. Q. Yuan, and M.-H. Fang, Europhys. Lett. **93**, 47004 (2011).

[35] S. M. Kazakov, A. M. Abakumov, S. Gonzlez, J. M. Perez-Mato, A. V. Ovchinnikov, M. V. Roslova, A. I. Boltalin, I. V. Morozov, E. V. Antipov, and G. Van Tendeloo, Chem. Mater. **23**, 4311 (2011).

[36] J. Q. Li, Y. J. Song, H. X. Yang, Z. Wang, H. L. Shi, G. F. Chen, Z. W. Wang, Z. Chen, and H. F. Tian, arXiv:1104.5340 (2011).

[37] I. Todorov, D. Y. Chung, H. Claus, C. D. Malliakas, A. P. Douvalis, T. Bakas, J. He, V. P. Dravid, and M. G. Kanatzidis, Chem. Mater. **22**, 3916 (2010).

[38] A. Iadecola, B. Joseph, L. Simonelli, A. Puri, Y. Mizuguchi, H. Takeya, Y. Takano, and N. L. Saini, J. Phys. Cond. Mat. **24**, 115701 (2012).

[39] T. Berlijn, P. J. Hirschfeld, and W. Ku, arXiv:1204.2849 (2012).

[40] A. Ricci, N. Poccia, G. Campi, B. Joseph, G. Arrighetti, L. Barba, M. Reynolds, M. Burghammer, H. Takeya, Y. Mizuguchi, Y. Takano, M. Colapietro, N. L. Saini, and A. Bianconi, Phys. Rev. B **84**, 060511 (2011).

[41] Z. Shermadini, H. Luetkens, R. Khasanov, A. Krzton-Maziopa, K. Conder, E. Pomjakushina, H.-H. Klauss, and A. Amato, Phys. Rev. B **85**, 100501 (2012).

[42] N. Lazarević, M. Abeykoon, P. W. Stephens, H. Lei, E. S. Bozin, C. Petrovic, and Z. V. Popović, Phys. Rev. B **86**, 054503 (2012).

[43] Y. Liu, Q. Xing, K. W. Dennis, R. W. McCallum, and T. A. Lograsso, arXiv:1208.4159 (2012).

[44] W. Bao, Q.-Z. Huang, G.-F. Chen, D.-M. Wang, J.-B. He, and Y.-M. Qiu, Chinese Phys. Lett. **28**, 086104 (2011).

[45] J. Sangster and A. Pelton, J. Phase Equil. **18**, 177 (1997).

[46] A. F. May, M. A. McGuire, H. Cao, I. Sergueev, C. Cantoni, B. C. Chakoumakos, D. S. Parker, and B. C. Sales, arXiv:1207.1318 (2012).

[47] B. C. Sales, M. A. McGuire, A. F. May, H. Cao, B. C. Chakoumakos, and A. S. Sefat, Phys. Rev. B **83**, 224510 (2011).

[48] B. Shen, B. Zeng, G. F. Chen, J. B. He, D. M. Wang, H. Yang, and H. H. Wen, Europhys. Lett. **96**, 37010 (2011).

[49] R. Liang, P. Dosanjh, D. Bonn, D. Baar, J. Carolan, and W. Hardy, Physica C **195**, 51 (1992).

[50] J. J. Ying, X. F. Wang, X. G. Luo, A. F. Wang, M. Zhang, Y. J. Yan, Z. J. Xiang, R. H. Liu, P. Cheng, G. J. Ye, and X. H. Chen, Phys. Rev. B **83**, 212502 (2011).

[51] W. Li, H. Ding, P. Deng, K. Chang, C. Song, K. He, L. Wang, X. Ma, J.-P. Hu, X. Chen, and Q.-K. Xue, Nature Phys. **8**, 126 (2012).

[52] M. Burrard-Lucas, D. G. Free, S. J. Sedlmaier, J. D. Wright, S. J. Cassidy, Y. Hara, A. J. Corkett, T. Lancaster, P. J. Baker, S. J. Blundell, and S. J. Clarke, arXiv:1203.5046 (2012).

[53] T. P. Ying, X. L. Chen, G. Wang, S. F. Jin, T. T. Zhou, X. F. Lai, H. Zhang, and W. Y. Wang, Sci. Rep. **2** (2012), 10.1038/srep00426.

[54] A. Krzton-Maziopa, E. V. Pomjakushina, V. Y. Pomjakushin, F. von Rohr, A. Schilling, and K. Conder, arXiv:1206.7022 (2012).

[55] J. R. Neilson and T. M. McQueen, J. Am. Chem. Soc. **134**, 7750 (2012).